

Decoherence of ensembles of nitrogen-vacancy centers in diamondErik Bauch,¹ Swati Singh,² Junghyun Lee ,^{3,4} Connor A. Hart,¹ Jennifer M. Schloss,^{3,5} Matthew J. Turner,^{1,5} John F. Barry,⁶ Linh M. Pham,⁶ Nir Bar-Gill,⁷ Susanne F. Yelin,^{1,8} and Ronald L. Walsworth^{1,5,9,*}¹*Department of Physics, Harvard University, Cambridge, Massachusetts 02138, USA*²*Electrical and Computer Engineering, University of Delaware, Newark, Delaware 19716, USA*³*Department of Physics, Massachusetts Institute of Technology, Cambridge, Massachusetts 02139, USA*⁴*Center for Quantum Information, Korea Institute of Science and Technology, Seoul 02792, Republic of Korea*⁵*Center for Brain Science, Harvard University, Cambridge, Massachusetts 02138, USA*⁶*Lincoln Laboratory, Massachusetts Institute of Technology, Lexington, Massachusetts 02420, USA*⁷*The Hebrew University of Jerusalem, Jerusalem 91904, Israel*⁸*Department of Physics, University of Connecticut, Storrs, Connecticut 06269, USA*⁹*Harvard-Smithsonian Center for Astrophysics, Cambridge, Massachusetts 02138, USA* (Received 24 June 2019; revised 13 July 2020; accepted 22 September 2020; published 23 October 2020)

We present a combined theoretical and experimental study of solid-state spin decoherence in an electronic spin bath, focusing specifically on ensembles of nitrogen-vacancy (NV) centers in diamond and the associated substitutional nitrogen spin bath. We perform measurements of NV spin free-induction decay (FID) times T_2^* and spin-echo coherence times T_2 in 25 diamond samples with nitrogen concentrations [N] ranging from 0.01 to 300 ppm. We introduce a microscopic model and perform numerical simulations to quantitatively explain the degradation of both T_2^* and T_2 over four orders of magnitude in [N]. Our analysis enables us to describe the NV ensemble spin coherence decay shapes as emerging consistently from the contribution of many individual NV centers.

DOI: [10.1103/PhysRevB.102.134210](https://doi.org/10.1103/PhysRevB.102.134210)**I. INTRODUCTION**

Solid-state spin systems have garnered increasing relevance as building blocks in a wide range of quantum science experiments [1–3]. Recently, high-sensitivity quantum sensing experiments have been enabled by nitrogen-vacancy (NV) spin ensembles in diamond [4–6]. Such work exploits NV centers' millisecond-long spin lifetimes under ambient conditions [7] and hinges on both the coherent microwave control and the optical initialization and readout of spin states. In addition to enabling technological advances [8–11], these favorable properties make NV centers, and specifically NV ensembles, a leading platform for the study of novel quantum many-body physics and nonequilibrium spin dynamics [12–14].

NV ensembles in diamond, like many solid-state spin systems, necessarily suffer from decay of coherence [with characteristic free-induction Ramsey decay (FID) time T_2^* and spin-echo decay time T_2] and spin state population (with time T_1). Dipolar interactions within the spin bath may limit these relaxation times, bounding the achievable sensitivity of NV-ensemble-based quantum sensing devices and revealing rich many-body dynamics of dipolar-coupled spin systems [see Fig. 1(a)] [15].

Solid-state spin-based sensing devices utilize host material widely ranging in concentrations of both electronic and nuclear spin species [4,14,16,17], which motivates investigation

of dipolar-induced decoherence across varying concentrations of both like and unlike spin species. For example, in NV-rich samples, paramagnetic substitutional nitrogen impurities (P1 centers, $S = 1/2$) [18–20] typically persist at concentrations similar to or exceeding the NV concentration, setting the NV spin-relaxation time scales. In other dense spin-ensemble systems, spin relaxation has been observed to be dominated by like-spin interactions [12,21,22].

Many factors contribute to the sensitivity of such quantum sensors. However, understanding the degree and character of T_2^* and T_2 decay is crucial for material engineering and designing spin interrogation schemes for high-performance quantum devices (see Ref. [23] for a detailed comparison). In this paper, we experimentally and theoretically investigate the NV dipolar-limited ensemble spin dephasing time T_2^* (measured through double-quantum coherence [14]) and the spin-echo coherence time T_2 in diamond samples with nitrogen density spanning more than four orders of magnitude. Our paper extends the comprehensive knowledge acquired for single NVs [17,24–26] to NV ensembles, and thus is critical for ensemble-based quantum applications.

II. EXPERIMENTAL RESULTS

Our study comprises 20 natural abundance diamond samples ($[^{12}\text{C}] = 1.1\%$, “ ^{12}C -samples”) and five isotopically enriched samples ($[^{13}\text{C}] \lesssim 0.05\%$, “ ^{12}C samples”) with total nitrogen concentrations in the range $[\text{N}] = 10$ ppb to 300 ppm.

*walsworth@umd.edu

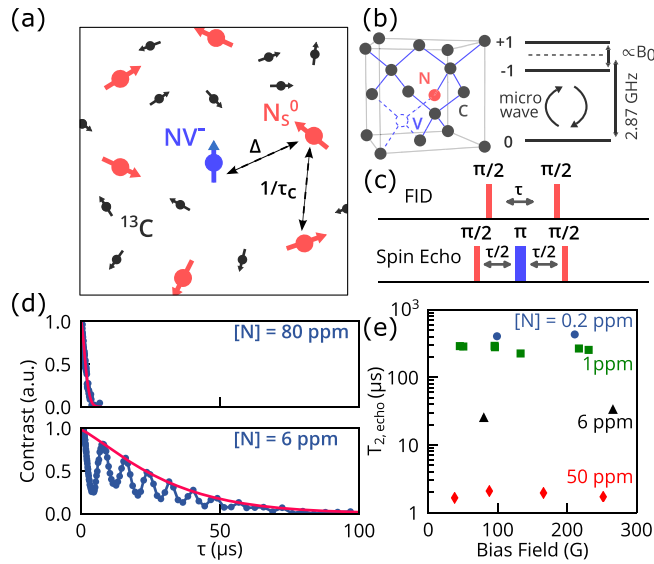


FIG. 1. (a) NV^- as central spin. (b) NV crystallographic defect and electronic spin-triplet ground-state level structure. (c) The free induction decay and spin-echo pulse sequence are used to measure T_2^* and T_2 , respectively. (d) Representative spin-echo decay fringes (blue) and envelope (red) for $[N] = 80$ - and 6-ppm diamond samples. (e) Magnetic field dependence of T_2 for a select set of samples.

In Fig. 1(d) we depict two spin-echo curves from diamonds with $[N] = 80$ and 6 ppm, which are representative of the set of 20 ^{13}C diamond samples studied in this paper. The data exhibit coherent modulation of the NV spin-echo signal due to Larmor precession of nuclear bath spins (see Appendix B) [27–29]. Isotopically enriched ^{12}C samples did not exhibit any modulation of the coherence signal irrespective of the applied magnetic field strength. The focus of this paper is the overall exponential-type decay, which is associated with loss of NV ensemble electronic spin coherence due to dipolar interactions with electronic nitrogen bath spins [25]. For all samples, the decay envelope was subsequently fitted to the form $C_0 \exp[-(t/T_2)^p]$ [red solid lines in Fig. 1(d)] to extract $T_2([N])$ and the stretched exponential parameter p [25,30].

Figure 1(e) shows T_2 times derived from this analysis for a select set of ^{12}C and ^{13}C samples as a function of magnetic bias field strengths. Only small variations in T_2 ($\lesssim 10\%$) are observable for the range of bias field strengths B_0 (2–30 mT, see Appendix B), indicating that T_2 is largely independent of magnetic field. Next, we summarize in Fig. 2(a) T_2 values for all samples as a function of nitrogen concentration $[N]$ with two regimes discernible. For $[N] \gtrsim 0.5$ ppm, T_2 exhibits an inverse-linear dependence on the nitrogen concentration, suggesting that interaction with nitrogen bath spins is the dominant source of decoherence of NV ensemble electronic spin. This inverse-linear scaling is consistent with studies in comparable crystalline systems and characteristic of dipolar-coupled spin environments [21,24,31,32]. In such instances, $1/T_2$ is proportional to the spin bath density n_{bath} , i.e., $1/T_2 = B \times n_{\text{bath}}$, where the factor B depends on microscopic details of the system-bath coupling and the spin bath dynamics.

For samples with $[N] \lesssim 0.5$ ppm, T_2 saturates at $\approx 700 \mu\text{s}$ for both isotopically purified and natural abundance samples.

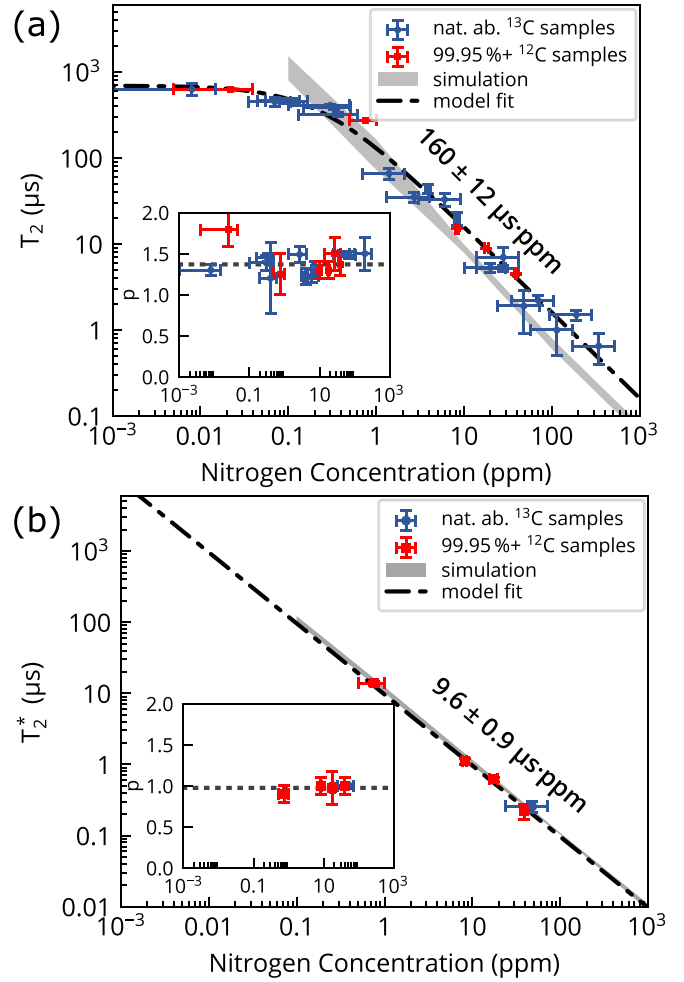


FIG. 2. (a) NV ensemble coherence time T_2 as a function of $[N]$ with orthogonal-distance regression fit to Eq. (1) (black dashed line) and range of values extracted from numerical simulation (gray band). Uncertainties are 95% confidence intervals. Inset: Stretched exponential parameters p with average value (black dotted line). T_2 measurements were taken with bias fields in the range of 2–30 mT (see Appendix B). (b) Similar fitting for NV ensemble dephasing time T_2^* . Measurements were taken at bias magnetic fields 2–3 mT at which any gradient-limited dephasing can be neglected.

This T_2 bound is below the observed limit of $T_{2,\text{max}} \approx T_1/2 \approx 2.5$ ms set by NV electronic spin lattice relaxation [33]. We attribute this limit to nitrogen-unrelated, quasistatic spurious magnetic noise [34,35] (see Appendix B) and additional paramagnetic spin defects in diamond. (In ^{13}C samples, the T_2 limit is set by ^{13}C nuclear spins to $\approx 600 \mu\text{s}$ [24,36]).

To further quantify the observed scaling, we fit the extracted T_2 values to the form

$$1/T_2([N]) = B_{\text{NV-N}} \times [N] + 1/T_{2,\text{other}}, \quad (1)$$

where $B_{\text{NV-N}}$ is the nitrogen-dominated NV decoherence rate per unit density and $T_{2,\text{other}}$ accounts for decoherence mechanisms independent of nitrogen. From the fit [black dashed line in Fig. 2(a)] we extract $B_{\text{NV-N}} = 2\pi \times (1.0 \pm 0.1)$ kHz/ppm ($1/B_{\text{NV-N}} = 160 \pm 12 \mu\text{s/ppm}$) and $T_{2,\text{other}} = 694 \pm 82 \mu\text{s}$. We also fit this model separately to the group of ^{13}C (blue dots) and ^{12}C (red squares) samples and find

agreement for $B_{\text{NV-N}}$ within error margins (see Appendix B). Suppression effects of the nitrogen spin bath due to ^{13}C nuclear spins [37] are indiscernible and neglected henceforth.

Additionally, we plot the extracted stretched exponential parameter p in the inset of Fig. 2(a). All samples exhibit exponential-type decay with a sample average $\bar{p} = 1.37 \pm 0.23$. This noninteger spin-echo decay is in striking contrast to the cubic decay ($p = 3$) observed for single NV centers [25,30] (see discussion below).

Similarly, FID Ramsey measurements were employed to determine the NV ensemble electronic spin dephasing time T_2^* ([N]). A recent related study [14] demonstrated that several dephasing mechanisms limit $T_2^* \lesssim 1\mu\text{s}$ in NV ensemble samples. Sources of ensemble dephasing include interactions with nuclear ^{13}C bath spins [14,24,38], crystal-lattice strain fields [14,39], and measurement-related artifacts such as magnetic field gradients and temperature fluctuations [14,40]. Great care was taken to isolate the nitrogen-specific contribution to T_2^* from other contributions. In particular, we limit our set of FID measurements to ^{12}C samples in the [N] = 1–100 ppm range for which ^{13}C -related dephasing can be neglected [14]. Moreover, we sense dephasing in the NV double quantum basis $\{+1, -1\}$ [14,41,42] to mitigate contributions from strain field gradients and temperature fluctuations in the samples. We correct for the twice higher dephasing rate in the double quantum basis; further details are provided in Appendix B and Ref. [14].

NV ensemble electronic spin dephasing times T_2^* and stretched exponential parameters p were extracted from the FID data by fitting decay envelopes to the form $C_0 \exp(-t/T_2^*)^p$. Figure 2(b) shows the measured T_2^* and p values as a function of [N] for the subset of samples. Similar to T_2 [Fig. 2(a)], we find T_2^* to scale inverse-linear with nitrogen concentration. We consequently fit the data to the form $1/T_2^*([\text{N}]) = A_{\text{NV-N}} \times [\text{N}]$ [compared to Eq. (1)], where $A_{\text{NV-N}}$ is the nitrogen-related NV ensemble dephasing rate per unit density. From the fit we extract $A_{\text{NV-N}} = 2\pi \times (16 \pm 1.5)$ kHz ppm ($1/A_{\text{NV-N}} = 9.6 \pm 0.9 \mu\text{s ppm}$). In addition, all FID NV ensemble measurements exhibit exponential decay [$p = 1$, see Fig. 2(b) inset], which deviates from the quadratic decay ($p = 2$) observed for single NV measurements [25,26].

III. THEORETICAL MODEL

We now present a phenomenological model for spin bath dynamics leading to the observed dephasing and decoherence. Under the secular approximation, the dipolar interaction between spins i and j can be simplified to [15]

$$H_{ij} = C_{\parallel}^{ij} S_z^i S_z^j + C_{\perp}^{ij} (S_+^i S_-^j + S_-^i S_+^j). \quad (2)$$

Transforming to a frame along the [111] crystal axis, the two coefficients are

$$C_{\parallel}^{ij} = \frac{\mu_0 \hbar^2 \mu_e^2}{4\pi r_{ij}^3} (1 - 2 \cos^2 \theta), \quad (3)$$

$$C_{\perp}^{ij} = \frac{\mu_0 \hbar^2 \mu_e^2}{4\pi 2r_{ij}^3} \left(1 - \frac{1}{4} \sin^2 \theta\right). \quad (4)$$

Here, r_{ij} is the distance, and θ is the angle between the applied magnetic field and the vector connecting the two

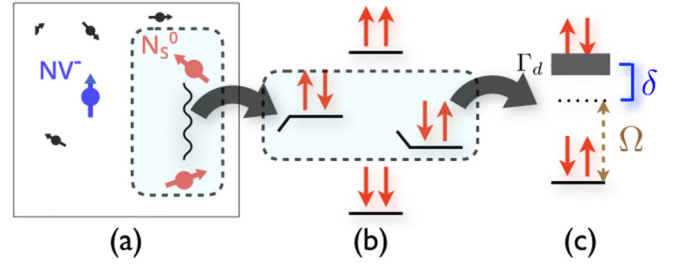


FIG. 3. Model for bath correlation time τ_c . (a) The bath spin dynamics arise due to interaction between nearby P1 spins. (b) States $|\uparrow\downarrow\rangle$ and $|\downarrow\uparrow\rangle$ give spin bath dynamics under Eq. (2). (c) Mapping to a spin-1/2 system.

spins. For dipolar interactions between NV and a P1 spin, the large NV zero field splitting makes flip-flop transitions non-energy-conserving and the second term in Eq. (2) is suppressed. The system-bath interaction simplifies to $H_{\text{NV-N}} = \sum_i C_{\parallel}^{\text{NV},i} S_z^{\text{NV}} S_z^i$, justifying treatment as an effective magnetic field the value of which depends on the state of bath spins. At room temperature, all spin states are equally occupied, allowing us to define interaction strength $\Delta^2 \equiv \sum_i (C_{\parallel}^{\text{NV},i})^2 / 4$ to characterize the effective magnetic field due to coupling between the NV spin and P1 bath spins. Δ quantifies the broadening of the NV sensor spin resonance and dephasing rate of the NV qubit.

We now evaluate the rate of P1 spin bath dynamics. In the presence of an external magnetic field, the flip-flop interaction between two P1 spins in Eq. (2) can be mapped to a pseudo-spin-1/2 system, with Hamiltonian $H_{\text{ps}} = \hbar\delta\sigma_z + \hbar\Omega\sigma_x$, where δ is the difference in the local field (including Overhauser) experienced by the two bath spins and $\Omega = C_{\perp}^{ij}$. As shown in Fig. 3, the pseudospin states $|e, g\rangle$ correspond to $|e\rangle = |\uparrow\downarrow\rangle$ and $|g\rangle = |\downarrow\uparrow\rangle$ states of the P1 spin pair. In numerically evaluating δ for simulations, we took into account the P1 nuclear spin state ($I = 1$), the P1 axis (along any of the four [111] diamond crystal axes) [43], and nearby P1 centers. Along with the coherent Hamiltonian evolution, there is a stochastic change in δ due to changes in the local spin environment caused by (among other things) flip-flop dynamics of far away bath spins. Including this incoherent part, the evolution of the density matrix is given by $\dot{\rho} = -i/\hbar[H_{\text{ps}}, \rho] + \mathcal{L}[\rho]$, where the Liouvillian includes dephasing at rate Γ_d . Here Γ_d denotes the rate of change of the effective magnetic field to which the pseudospin is subjected. Solving for the rate of change of population (R_{flip}^{ij}), we obtain

$$R_{\text{flip}}^{ij} = \frac{\Omega^2}{\Gamma_d} \frac{\Gamma_d^2}{\Gamma_d^2 + \delta^2}. \quad (5)$$

Assuming all P1 spin pairs act independently, the overall rate of bath dynamics becomes $R_{\text{Tot}} = \sum_{\{i,j\}} R_{\text{flip}}^{ij}$. Realistically, each spin pair has a different δ and Γ_d . Nonetheless, while we evaluated δ for each P1 spin numerically, we assumed all pairs have the same $\Gamma_d \approx \sqrt{N_b} \bar{C}_{\parallel}^{ij}$, where N_b is the number of bath spins and \bar{C}_{\parallel}^{ij} is the average dipolar interaction. Note that Γ_d is the intrinsic linewidth of the dipolar spin bath [44]. We define the spin bath correlation time $\tau_c \equiv 1/R_{\text{Tot}}$.

While the origins of Δ and τ_c are quantum in nature, in order to estimate the coherence properties of NV ensembles, we model the P1 bath dynamics as an effective random magnetic field with root-mean-square strength Δ and correlation time τ_c [25,30]. This approximation works well due to the low density of impurity spins and slow bath dynamics, allowing us to ignore higher-order quantum effects. In our model for the NV spin coherence signal, the effect of the P1 bath is modeled as an Ornstein-Uhlenbeck stochastic process [30,45,46].

For a single NV initially polarized in the $|0\rangle$ state and undergoing $|0\rangle \leftrightarrow |-1\rangle$ (or $|0\rangle \leftrightarrow |+1\rangle$) transition, the probability to be in state $|0\rangle$ after time $t \ll \tau_c$ is given by $p_{\text{FID}}^{\text{single}}(t) = \frac{1}{2}[1 + e^{-(t/T_{2,\text{single}}^*)^2}]$ and $p_{\text{echo}}^{\text{single}}(t) = \frac{1}{2}[1 + e^{-(t/T_{2,\text{single}})^3}]$ [25,30] (see Appendix C) for the FID and spin-echo scheme, respectively. Here, $T_{2,\text{single}}^* = \sqrt{2}/\Delta_{\text{single}}$ and $T_{2,\text{single}} = (12\tau_{c,\text{single}}/\Delta_{\text{single}}^2)^{1/3}$, where (as discussed previously) Δ_{single} characterizes the system-bath coupling and $\tau_{c,\text{single}}$ characterizes the spin bath correlation time. In order to evaluate NV ensemble averaged probabilities, we need to integrate $p_{\text{FID}}^{\text{single}}$ and $p_{\text{echo}}^{\text{single}}$ over a distribution of various Δ_{single} and $\tau_{c,\text{single}}$.

For dipolar interactions, the probability density function (PDF) for Δ_{single} has the form

$$P(\Delta_{\text{single}}) = \frac{\Delta_{\text{ens}}}{\Delta_{\text{single}}^2} \sqrt{\frac{2}{\pi}} e^{-\Delta_{\text{ens}}^2/2\Delta_{\text{single}}^2}, \quad (6)$$

where Δ_{ens} is the average spin-spin coupling strength within the NV ensemble [47]. Integrating $p_{\text{FID}}^{\text{single}}(t)$ over the distribution of Δ_{single} , we arrive at the ensemble averaged probability:

$$p_{\text{FID}}^{\text{ens}}(t) = \frac{1}{2}[1 + e^{-(t/T_{2,\text{ens}}^*)^2}], \quad (7)$$

where $T_{2,\text{ens}}^* = 1/\Delta_{\text{ens}}$. The ensemble-averaged NV FID signal exhibits simple exponential decay ($p = 1$) in agreement with experimental results [see Fig. 2(b) inset].

A similar analysis can be done for NV ensemble T_2 , while also accounting for the distribution of $\tau_{c,\text{single}}$. In our classical treatment, τ_c can be interpreted as a first passage time for a stochastic process (here several bath spin flip-flops) with the PDF:

$$P(\tau_{c,\text{single}}) = \sqrt{\frac{\lambda}{2\pi\tau_{c,\text{single}}^3}} e^{-\frac{\lambda(\tau_{c,\text{single}} - \tau_{c,\text{ens}})^2}{2\tau_{c,\text{single}}\tau_{c,\text{ens}}^2}}. \quad (8)$$

Here, λ and $\tau_{c,\text{ens}}$ are the shape parameter and the ensemble mean of the distribution, respectively [48]. We integrate over the PDFs of Δ_{single} and $\tau_{c,\text{single}}$ to obtain

$$p_{\text{echo}}^{\text{ens}}(t) \approx \frac{1}{2}[1 + e^{-(t/T_{2,\text{ens}})^{3/2}}], \quad (9)$$

where $T_{2,\text{ens}} = (2\tau_{c,\text{ens}}/\Delta_{\text{ens}}^2)^{1/3}$ ($t \ll \tau_{c,\text{ens}}$). The ensemble-averaged spin-echo decay exhibits noninteger decay with $p \approx 3/2$, in agreement with measured ensemble spin-echo decay envelopes [see Fig. 2(a) inset].

Figure 4 shows the distribution of Δ_{single} and $\tau_{c,\text{single}}$ for 10^4 NV spin bath simulations for $[N] = 100$ ppm, along with the fitted ensemble PDF. For each nitrogen concentration, we choose 10^4 realizations to have sufficient statistics capturing the long tail region of the PDFs. From these PDF fits,

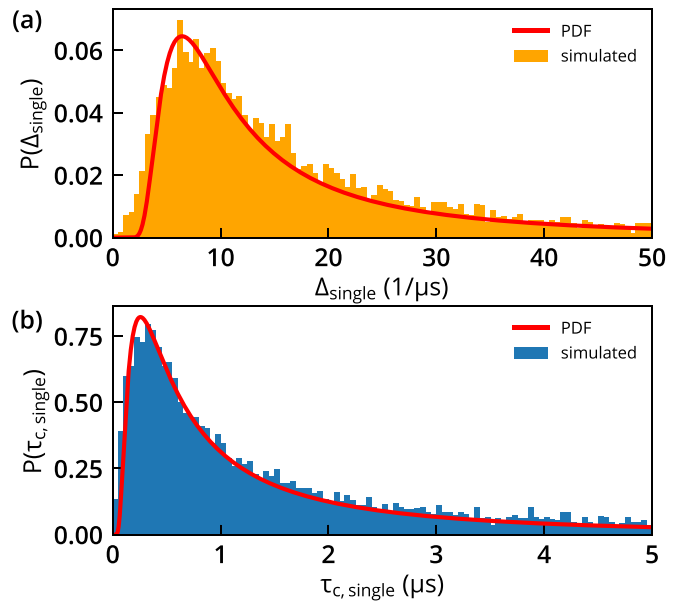


FIG. 4. Simulated distribution of coupling strength Δ (a) and bath correlation time τ_c (b) for $[N] = 100$ ppm extracted from 10^4 spin bath configurations.

we extract values of Δ_{ens} and $\tau_{c,\text{ens}}$. By using these extracted values in Eqs. (7) and (9), we connect our classical stochastic model for ensemble averaging a noisy magnetic field with our microscopic model for spin bath dynamics, thereby obtaining the scaling with $[N]$. The range of T_2^* and T_2 values produced due to fit uncertainty is depicted in Fig. 2 as a gray band, showing good agreement with experiments. We emphasize that the gray curves in Fig. 2 involve no fitting parameters unlike earlier works [25,26]. Our parameter-free simulation for T_2 is less accurate than for T_2^* . Unlike T_2^* , T_2 depends on the many-body dynamics of the spin bath, and mean field models like the stochastic one used here are insufficient to accurately capture dynamics of such disordered quantum systems. While adding a stochastic treatment of $\tau_{c,\text{single}}$, our results are consistent with earlier predictions regarding classical modeling of spin baths [46].

Finally, in Table I we compare the p parameters observed in the present and other NV spin-resonance experiments. For single NVs in nitrogen-rich diamonds (and related systems), the experimentally observed decay shapes for FID, spin-echo, and spin-lifetime measurements have been well explained by theory (Table I, column 2).

TABLE I. Summary of the stretched exponential parameter p in single NV and NV ensemble measurements determined through experiment and theory.

Experiment	Single NV		NV ensemble	
	p	Expt./Theor.	p	Expt./Theor.
T_2	3	[25]/[30]	$\approx 3/2$	This paper
T_2^*	2	[25]/[30]	1	[14]/[49], this paper
T_1 (cross-relax.)			1/2	[12,50]/[12,51]
T_1 (spin-lattice)	1	[52]	1	[53,54]

However, as has been observed in several previous NV ensemble experiments, when averaging the decay signal of many individual NVs with slightly varying spin environments, new decay shapes with *reduced* shape parameters emerge (Table I, column 3). Our paper completes the mapping of decay shapes observed in single-NV experiments to that of NV ensembles.

IV. CONCLUSION AND OUTLOOK

We measured the T_2^* and T_2 decay for NV ensembles as a function of nitrogen concentration over several orders of magnitude, demonstrating stretched exponential decay ensemble coherence. Our data indicate that lower nitrogen concentration leads to longer T_2^* and T_2 times, until nitrogen independent decoherence mechanisms start dominating. However, lower nitrogen concentration also leads to a reduced signal for most applications, such as magnetometry. Reference [23] provides a detailed discussion of various factors involved in ensemble NV sensitivity optimization for magnetometry applications, including nitrogen concentration.

We also showed that qualitative features of the ensemble coherence signal are well modeled by a classical stochastic process, with T_2 power scaling of 3/2 emerging from integrating over single NVs centers. We connected this classical treatment to a microscopic quantum model for the bath correlation time using numerical simulations; and found reasonable agreement with experiments with no fitting parameters. While our model describes the relevant scalings and coherence decay shapes, the underestimation of T_2 , particularly for larger concentrations, may indicate localization-type behavior. Future work would include investigation of localized phases in these systems.

ACKNOWLEDGMENTS

We acknowledge fruitful discussion with Joonhee Choi and Soonwon Choi. We thank Evans Analytical Group (EAG) Laboratories for the secondary ion mass spectroscopy measurements of nitrogen concentration. This material is based upon work supported by, or in part by, the US Army Research Laboratory and the U.S. Army Research Office under Grant No. W911NF1510548; the NSF Electronics, Photonics, and Magnetic Devices program under Grant No. ECCS-1408075; the NSF Physics of Living Systems program under Grant No. PHY-1504610; the Integrated NSF Support Promoting Interdisciplinary Research and Education program under Grant No. EAR-1647504; and Lockheed Martin under Grant No. A32198. This work was performed in part at the Center for Nanoscale Systems, a member of the National Nanotechnology Coordinated Infrastructure Network, which is supported by the NSF under Grant No. 1541959. J.M.S. was supported by a Fannie and John Hertz Foundation Graduate Fellowship and a NSF Graduate Research Fellowship under Grant No. 1122374.

APPENDIX A: SAMPLE CHARACTERIZATION

All diamond crystals were manufactured by Element Six and Apollo Diamond [55]. Samples with nitrogen spin densities $[N] \lesssim 100$ ppm were grown using chemical vapor deposition (CVD; for a review, see Ref. [56]) and consist of

bulk diamond plates, as well as thin ($\lesssim 100 \mu\text{m}$) nitrogen-doped layers grown on top of Ib or IIa diamond substrates. Two other samples were grown using the high-pressure high-temperature (HPHT) method [57–61] and cover the range $[N] \gtrsim 100$ ppm. We purposefully choose diamond samples with grown-in spin concentrations $[NV] \ll [N]$ to limit the study to NV decoherence resulting from paramagnetic nitrogen bath spins. NV-NV dipolar interactions are thus negligible for the experiments in this paper.

The total nitrogen concentration within diamond samples studied in this paper is determined by several methods: For the majority of samples, the manufacturers provided estimated nitrogen spin concentrations or secondary ion mass spectroscopy (SIMS) data taken on samples from the same growth run. In addition, for a subset of samples SIMS measurements were performed by EAG Laboratories. In select samples, nitrogen was determined through Fourier-transformed infrared spectroscopy [60,62].

The reported uncertainties in $[N]$ are calculated from the mean and variation in spin concentration values provided by combining results from various methods. If only one method was available, the uncertainty is given by the method's reported error margin. For SIMS measurements an error of 50% is conservatively assumed, which also accounts for variations in N throughout different parts of a sample.

Taking the ratio $T_2([N])/T_2^*([N]) = A_{NV-N}/B_{NV-N}$, which is independent of absolute nitrogen concentration, we find that T_2 exceeds T_2^* by a factor of ≈ 16 across a wide range of diamond samples and $[N]$. Given the provided scalings, calibration of bulk substitutional nitrogen spin concentrations through NV coherence measurements can thus be performed and is routinely used in our laboratory. We emphasize that the role of the ^{13}C bath is negligible if nitrogen is the dominant source of NV ensemble electronic spin decoherence.

APPENDIX B: MEASUREMENT DETAILS

For our measurements we deployed confocal and wide-field NV microscopy. In both setups, 532-nm laser light is applied to optically initialize and readout the NV spin polarization. In addition, we apply a static magnetic field B_0 along one of the $[111]$ crystal directions (misalignment angle $\leq 3^\circ$), which singles out one of the four possible NV orientations and lifts the $|\pm 1\rangle$ degeneracy of the NV spin-1 ground state [see Fig. 1(b)]. Pulsed microwaves resonant with the $|0\rangle \leftrightarrow |-1\rangle$ or $|0\rangle \leftrightarrow |+1\rangle$ spin transition are deployed to coherently manipulate the NV spin state.

1. Spin echo

Low nitrogen density ^{13}C samples exhibited periodic modulation of the NV spin-echo signal (electron spin echo envelope modulation, Refs. [27,28]) owing to the Larmor precession of the ^{13}C nuclear spin bath, as shown in Fig. 1(d) ($[N] = 6$ -ppm sample). Revival and collapses of the spin-echo signal occurred with frequency $f_{\text{Larmor}} = \frac{\gamma_{^{13}\text{C}}}{2\pi} B_0$, where $\gamma_{^{13}\text{C}} = 2\pi \times 1.07 \text{ MHz/T}$ [28,29] is the ^{13}C nuclear gyromagnetic ratio and B_0 is the bias magnetic field. To clearly separate the overall decay envelope from the Larmor signal, for each natural abundance ^{13}C sample the bias field was adjusted

between 2 and 30 mT to tune the Larmor precession frequency such that $f_{\text{Larmor}} \gg 1/T_2$ (low nitrogen samples) or $f_{\text{Larmor}} \ll 1/T_2$ (high nitrogen samples). The isotopically enriched ^{12}C samples did not exhibit modulation of the coherence signal independent of the applied magnetic field strength. As discussed in the main text and Fig. 1(e), only small variations in NV T_2 are observed with changing B_0 , which suggests that T_2 is largely independent of bias magnetic field for the range of fields.

We also fit Eq. (1) to the ^{13}C and ^{12}C sample NV T_2 data alone [see Fig. 2(a)] and obtained $\{B_{\text{NV-N}} = 2\pi \times (1.0 \pm 0.2) \text{ kHz/ppm}, T_{2,\text{other}} = 715 \pm 248 \mu\text{s}\}$ and $\{B_{\text{NV-N}} = 2\pi \times (0.9 \pm 0.1) \text{ kHz/ppm}, T_{2,\text{other}} = 657 \pm 94 \mu\text{s}\}$, respectively. The close agreement (within error margins) among $B_{\text{NV-N}}$ values extracted for ^{13}C , ^{12}C , and the combined data suggests that NV spin ensemble decoherence due to ^{13}C nuclear spins in natural abundance samples on T_2 is negligible, when nitrogen is the dominant source of decoherence.

2. Ramsey

Several inhomogeneous broadening mechanisms contribute to NV ensemble spin dephasing. For example, the T_2^* limit in natural abundance samples set by 1.1% ^{13}C spins ($\approx 1 \mu\text{s}$ [14]) restricts our measurements to isotopically enriched ^{12}C samples. In addition, FID decay was probed in the NV center's double quantum basis ($\{-1, +1\}$) to mitigate effects of strain fields and temperature fluctuations. To account for the twice higher gyromagnetic ratio and doubled dephasing rate in the double quantum basis, the extracted T_2^* values are multiplied by 2. Lastly, measurements were performed at low magnetic bias fields ($\lesssim 20 \text{ G}$) to reduce the influence of magnetic field gradients. Further experimental details are given in Ref. [14].

3. T_2 limit at low [N]

Samples were sourced from multiple growers to minimize effects intrinsic to a single grower's manufacturing process. In addition, samples were repeatedly measured in multiple setups to minimize experimental error. We attribute the observed T_2 limit at the lowest nitrogen concentrations to spurious, low-frequency ambient magnetic noise. Such effects are especially pernicious in the spin-echo measurements employed in this paper, given the long coherence times of our low nitrogen samples (approximately milliseconds). In addition, it is well known that secondary paramagnetic spin species are incorporated into the crystal at elevated concentrations during CVD and HPHT diamond growth. Importantly, such decoherence mechanisms are not expected to scale with nitrogen concentration and can thus be accounted for in our model via $T_{2,\text{other}}$.

APPENDIX C: CLASSICAL TREATMENT OF THE SPIN BATH DYNAMICS

In this section, we discuss the evolution of several standard pulse sequences on an NV electronic spin in the presence of a fluctuating magnetic field. We also perform ensemble averages over a distribution of NV centers in order to evaluate the form of experimentally measured signals.

For an NV center undergoing dynamical decoupling pulse sequences under the presence of a fluctuating magnetic field, the probability to find the NV electronic spin in state $|0\rangle$ after time τ is given by

$$p(\tau) = \frac{1}{2}[1 + \langle \cos \phi(\tau) \rangle] = \frac{1}{2}(1 + \text{Re}[\langle e^{i\phi(\tau)} \rangle]). \quad (\text{C1})$$

Here, the total phase difference accumulated is

$$\phi(t) = \frac{g\mu_B}{\hbar} \int dt f(t)B(t), \quad (\text{C2})$$

where $f(t)$ are steplike functions describing the periodic inversion of the NV spin for the pulse sequence under consideration [30,63], and $B(t)$ includes the random magnetic fields due to the spin bath surrounding the NV center.

Considering we have a large number of impurity spins with different couplings to the NV center, we assume that the random fluctuating magnetic field due to the spin bath has a Gaussian distribution (with zero mean), simply due to the central limit theorem [25]. Invoking properties of Gaussian noise, Eq. (C1) simplifies to

$$p(\tau) = \frac{1}{2}(1 + e^{-(\phi(\tau)^2)/2}) = \frac{1}{2}(1 + e^{-\chi(\tau)}), \quad (\text{C3})$$

where

$$\chi(\tau) = \left(\frac{g\mu_B}{\hbar}\right)^2 \int \frac{d\omega}{2\pi} \frac{S_B(\omega)}{\omega^2} F(\omega\tau). \quad (\text{C4})$$

Following the convention established by Ref. [63] and others,

$$S_B = \int dt e^{i\omega t} \langle B(t)B(0) \rangle \quad (\text{C5})$$

is the classical magnetic field spectral noise density and

$$F(\omega\tau) = \frac{\omega^2}{2} |\tilde{f}(\omega)|^2 \quad (\text{C6})$$

is the filter function of the pulse sequence under consideration. The properties of the random magnetic field imposed here make it equivalent to treating it as an Ornstein-Uhlenbeck stochastic process [25,30,45,46].

We now look into the microscopic origin of the fluctuating magnetic field. For a bath spin Larmor precessing at ω_L , the effective magnetic field at the central spin is given by $B_1 \cos(\omega_L t)$. Assuming the coherent spin precession decays at a timescale characterized by the bath correlation time τ_c , the magnetic field at the central spin can be approximated by $B(t) = B_1 \cos(\omega_L t) e^{-t/\tau_c}$. Thus the bath spectral density becomes

$$\begin{aligned} S_B[\omega] &= \int dt e^{i\omega t} \langle B_1^2 \rangle \cos(\omega_L t) e^{-t/\tau_c} \\ &= \left[\frac{\tau_c \langle B_1^2 \rangle}{1 + (\omega - \omega_L)^2 \tau_c^2} + \frac{\tau_c \langle B_1^2 \rangle}{1 + (\omega + \omega_L)^2 \tau_c^2} \right]. \end{aligned} \quad (\text{C7})$$

In the short-time (high-frequency) limit, the bath spectral density function can be simplified to

$$S_B[\omega] \approx \langle B_1^2 \rangle \tau_c \frac{2}{1 + (\delta\tau_c)^2}, \quad (\text{C8})$$

where $\delta = (\omega - \omega_L)$. For brevity and consistency with the main text, we define $\Delta_{\text{single}}^2 \equiv (g\mu_B/\hbar)^2 \langle B_1^2 \rangle$. For an NV free-induction decay measurement, the filter function is given by

$F(\omega\tau) = 2 \sin^2(\omega\tau/2)$ [63], leading to

$$\begin{aligned}\chi_{\text{FID}}(\tau) &= \frac{2}{\pi} \Delta_{\text{single}}^2 \tau_c \int \frac{d\omega}{\omega^2} \frac{1}{1 + (\delta\tau_c)^2} \sin^2(\omega\tau/2) \\ &= \Delta_{\text{single}}^2 \tau_c^2 \left[\frac{t}{\tau_c} - 1 + e^{-t/\tau_c} \right].\end{aligned}\quad (\text{C9})$$

For a spin-echo measurement, the filter function is given by $F(\omega\tau) = 8 \sin^4(\omega\tau/4)$ [63], giving us

$$\begin{aligned}\chi_{\text{SE}}(\tau) &= \frac{8}{\pi} \Delta_{\text{single}}^2 \tau_c \int \frac{d\omega}{\omega^2} \frac{1}{1 + (\delta\tau_c)^2} \sin^4(\omega\tau/4) \\ &= \Delta_{\text{single}}^2 \tau_c^2 \left[\frac{t}{\tau_c} - 3 - e^{-t/\tau_c} + 4e^{-t/2\tau_c} \right].\end{aligned}\quad (\text{C10})$$

For short times, i.e., $t \ll \tau_c$ (but $\Delta_{\text{single}} \tau_c \gg 1$), χ for the two measurements simplifies to

$$\begin{aligned}\chi_{\text{FID}}(\tau) &\approx \frac{\Delta_{\text{single}}^2}{2} t^2, \\ \chi_{\text{SE}}(\tau) &\approx \frac{\Delta_{\text{single}}^2}{12\tau_c} t^3.\end{aligned}\quad (\text{C11})$$

Substituting this in Eq. (C3), we get

$$p_{\text{FID}}^{\text{single}}(t) = \frac{1}{2} (1 + e^{-(t/T_{2,\text{single}}^*)^2}), \quad (\text{C12})$$

$$p_{\text{SE}}^{\text{single}}(t) = \frac{1}{2} (1 + e^{-(t/T_{2,\text{single}})^3}), \quad (\text{C13})$$

where

$$T_{2,\text{single}}^* = \left[\frac{2}{\Delta_{\text{single}}^2} \right]^{1/2}, \quad (\text{C14})$$

$$T_{2,\text{single}} = \left[\frac{12\tau_{c,\text{single}}}{\Delta_{\text{single}}^2} \right]^{1/3}. \quad (\text{C15})$$

Here, we have replaced τ_c with $\tau_{c,\text{single}}$ to be consistent with the main text. Finally, comparing this with the phenomenological quantum model of the spin bath dynamics developed in this paper, we get

$$\Delta_{\text{single}}^2 = \sum_i (C_{\parallel}^{\text{NV},i}/2)^2, \quad (\text{C16})$$

$$\frac{1}{\tau_{c,\text{single}}} = \sum_{\text{P1},\{i,j\}} R_{\text{flip}}^{ij}. \quad (\text{C17})$$

The time dependencies for various dynamical decoupling protocols become different if we average this signal over several NV centers, each evolving under a random spin bath distribution, as in experiments. For dipolar interactions, the

probability density function for Δ_{single} has the form [47]

$$P(\Delta_{\text{single}}) = \frac{\Delta_{\text{ens}}}{\Delta_{\text{single}}^2} \sqrt{\frac{2}{\pi}} e^{-\Delta_{\text{ens}}^2/2\Delta_{\text{single}}^2}. \quad (\text{C18})$$

Here, Δ_{ens} is the average coupling strength of the NV to the spin bath within the NV ensemble. Integrating $p_{\text{FID}}^{\text{single}}(t)$ over the distribution of Δ_{single} , we arrive at the ensemble averaged probability:

$$p_{\text{FID}}^{\text{ens}}(t) = \frac{1}{2} [1 + e^{-(t/T_{2,\text{ens}}^*)^2}], \quad (\text{C19})$$

where $T_{2,\text{ens}}^* = 1/\Delta_{\text{ens}}$. The ensemble averaged FID signal thus exhibits simple exponential decay ($p = 1$) in agreement with our experimental results [see Fig. 2(b) inset].

We now perform a similar analysis to get an expression for the ensemble-averaged NV decoherence time $T_{2,\text{ens}}$. In this case, we need to take into account the nitrogen electronic spin bath dynamics. We classically model the bath correlation time as the time taken for a stochastic process (here several bath spin flip-flops) to reach a certain threshold, thus $\tau_{c,\text{single}}$ can be seen as the equivalent of first passage time. The probability distribution function of τ_c here is assumed to be a simplified Gaussian PDF given by

$$P(\tau_{c,\text{single}}) = \sqrt{\frac{\lambda}{2\pi\tau_{c,\text{single}}^3}} e^{-\lambda(\tau_{c,\text{single}} - \tau_{c,\text{ens}})^2/2\tau_{c,\text{single}}\tau_{c,\text{ens}}^2}. \quad (\text{C20})$$

Here, λ is an overall fitting parameter, and $\tau_{c,\text{ens}}$ is the ensemble mean of the distribution. Integrating over the distributions of Δ_{single} and $\tau_{c,\text{single}}$, we get for the spin-echo signal

$$p_{\text{SE}}^{\text{ens}}(t) \approx \frac{1}{2} [1 + e^{-(t/T_{2,\text{ens}})^{3/2}}], \quad (\text{C21})$$

where $T_{2,\text{ens}} = (2\tau_{c,\text{ens}}/\Delta_{\text{ens}}^2)^{1/3}$, and the ensemble-averaged decay exhibits noninteger decay with $p \approx 3/2$.

APPENDIX D: NUMERICAL SIMULATIONS

In order to simulate a random mixed electronic spin bath and its dynamics, we start with a diamond lattice putting an NV at origin, and pick random lattice sites for nitrogen P1 centers with the right concentration. Current simulations include 0.1–1000 ppm of nitrogen spins. We evaluate the dipole-dipole interaction between the NV and P1 spins to obtain Δ_{single} given by Eq. (C16). To obtain $\tau_{c,\text{single}}$, we sum all the P1 spin-pair interactions according to Eq. (C17). Finally, we extract the ensemble averaged values Δ_{ens} and $\tau_{c,\text{ens}}$ from the distribution generated from $\approx 10^4$ bath realizations (see Fig. 4 in the main text for [N = 100 ppm]). When numerically estimating $\tau_{c,\text{single}}$, we ignore spin bath pairs that interact weakly with the NV, leading to motional narrowing, as discussed in literature [25,30].

- [1] K. Saedi, S. Simmons, J. Z. Salvail, P. Dluhy, H. Riemann, N. V. Abrosimov, P. Becker, H.-J. Pohl, J. J. L. Morton, and M. L. W. Thewalt, *Science* **342**, 830 (2013).
 [2] B. Hensen, H. Bernien, A. E. Dréau, A. Reiserer, N. Kalb, M. S. Blok, J. Ruitenberg, R. F. L. Vermeulen, R. N. Schouten, C. Abellán, W. Amaya, V. Pruneri, M. W. Mitchell, M. Markham,

D. J. Twitchen, D. Elkouss, S. Wehner, T. H. Taminiau, and R. Hanson, *Nature (London)* **526**, 682 (2015).

- [3] A. Sipahigil, R. E. Evans, D. D. Sukachev, M. J. Burek, J. Borregaard, M. K. Bhaskar, C. T. Nguyen, J. L. Pacheco, H. A. Atikian, C. Meuwly, R. M. Camacho, F. Jelezko, E. Bielejec, H. Park, M. Lončar, and M. D. Lukin, *Science* **354**, 847 (2016).

- [4] T. Wolf, P. Neumann, K. Nakamura, H. Sumiya, T. Ohshima, J. Isoya, and J. Wrachtrup, *Phys. Rev. X* **5**, 041001 (2015).
- [5] J. F. Barry, M. J. Turner, J. M. Schloss, D. R. Glenn, Y. Song, M. D. Lukin, H. Park, and R. L. Walsworth, *Proc. Natl. Acad. Sci. USA* **113**, 14133 (2016).
- [6] G. Chatzidrosos, A. Wickenbrock, L. Bougas, N. Leefer, T. Wu, K. Jensen, Y. Dumeige, and D. Budker, *Phys. Rev. Appl.* **8**, 044019 (2017).
- [7] M. W. Doherty, N. B. Manson, P. Delaney, F. Jelezko, J. Wrachtrup, and L. C. L. Hollenberg, *Phys. Rep.* **528**, 1 (2013).
- [8] P. Frontera, S. Alessandrini, and J. Stetson, in Proceedings of the IEEE/ION Position, Location, and Navigation Symposium, 2018 (unpublished), p. 497.
- [9] D. R. Glenn, D. B. Bucher, J. Lee, M. D. Lukin, H. Park, and R. L. Walsworth, *Nature (London)* **555**, 351 (2018).
- [10] J. D. Breeze, E. Salvadori, J. Sathian, N. M. N. Alford, and C. W. Kay, *Nature (London)* **555**, 493 (2018).
- [11] E. V. Levine, M. J. Turner, P. Kehayias, C. A. Hart, N. Langellier, R. Trubko, D. R. Glenn, R. R. Fu, and R. L. Walsworth, *Nanophotonics* **8**, 1945 (2019).
- [12] J. Choi, S. Choi, G. Kucsko, P. C. Maurer, B. J. Shields, H. Sumiya, S. Onoda, J. Isoya, E. Demler, F. Jelezko, N. Y. Yao, and M. D. Lukin, *Phys. Rev. Lett.* **118**, 093601 (2017).
- [13] S. Choi, J. Choi, R. Landig, G. Kucsko, H. Zhou, J. Isoya, F. Jelezko, S. Onoda, H. Sumiya, V. Khemani, C. von Keyserlingk, N. Y. Yao, E. Demler, and M. D. Lukin, *Nature (London)* **543**, 221 (2017).
- [14] E. Bauch, C. A. Hart, J. M. Schloss, M. J. Turner, J. F. Barry, P. Kehayias, S. Singh, and R. L. Walsworth, *Phys. Rev. X* **8**, 031025 (2018).
- [15] A. Abragam, *The Principles of Nuclear Magnetism* (Clarendon, Oxford, 1983), p. 599.
- [16] V. M. Acosta, E. Bauch, M. P. Ledbetter, C. Santori, K. M. C. Fu, P. E. Barclay, R. G. Beausoleil, H. Linget, J. F. Roch, F. Treussart, S. Chemerisov, W. Gawlik, and D. Budker, *Phys. Rev. B* **80**, 115202 (2009).
- [17] G. Balasubramanian, P. Neumann, D. Twitchen, M. Markham, R. Kolesov, N. Mizuochi, J. Isoya, J. Achard, J. Beck, J. Tissler, V. Jacques, P. R. Hemmer, F. Jelezko, and J. Wrachtrup, *Nature Materials* **8**, 383 (2009).
- [18] W. V. Smith, P. P. Sorokin, I. L. Gelles, and G. J. Lasher, *Phys. Rev.* **115**, 1546 (1959).
- [19] R. J. Cook and D. H. Whiffen, *Proc. R. Soc. A* **295**, 99 (1966).
- [20] J. H. N. Loubser and J. A. v. Wyk, *Rep. Prog. Phys.* **41**, 1201 (1978).
- [21] J. A. Van Wyk, E. C. Reynhardt, G. L. High, and I. Kiflawi, *J. Phys. D* **30**, 1790 (1997).
- [22] A. M. Tyryshkin, S. Tojo, J. J. L. Morton, H. Riemann, N. V. Abrosimov, P. Becker, H.-J. Pohl, T. Schenkel, M. L. W. Thewalt, K. M. Itoh, and S. A. Lyon, *Nat. Mater.* **11**, 143 (2012).
- [23] J. F. Barry, J. M. Schloss, E. Bauch, M. J. Turner, C. A. Hart, L. M. Pham, and R. L. Walsworth, *Rev. Mod. Phys.* **92**, 015004 (2000).
- [24] N. Mizuochi, P. Neumann, F. Rempp, J. Beck, V. Jacques, P. Siyushev, K. Nakamura, D. J. Twitchen, H. Watanabe, S. Yamasaki, F. Jelezko, and J. Wrachtrup, *Phys. Rev. B* **80**, 041201 (2009).
- [25] G. de Lange, Z. H. Wang, D. Riste, V. V. Dobrovitski, and R. Hanson, *Science* **330**, 60 (2010).
- [26] G. de Lange, T. van der Sar, M. Blok, Z.-H. Wang, V. Dobrovitski, and R. Hanson, *Scientific Reports* **2**, 382 (2012).
- [27] L. Rowan, E. Hahn, and W. Mims, *Phys. Rev.* **137**, A61 (1965).
- [28] L. Childress, M. V. Gurudev Dutt, J. M. Taylor, A. S. Zibrov, F. Jelezko, J. Wrachtrup, P. R. Hemmer, and M. D. Lukin, *Science* **314**, 281 (2006).
- [29] P. L. Stanwix, L. M. Pham, J. R. Maze, D. Le Sage, T. K. Yeung, P. Cappellaro, P. R. Hemmer, A. Yacoby, M. D. Lukin, and R. L. Walsworth, *Phys. Rev. B* **82**, 201201 (2010).
- [30] R. de Sousa, in *Electron Spin Resonance and Related Phenomena in Low-Dimensional Structures*, edited by M. Fanciulli, Topics in Applied Physics Vol. 115 (Springer-Verlag, Berlin, 2009), pp. 183–220.
- [31] E. Abe, A. M. Tyryshkin, S. Tojo, J. J. Morton, W. M. Witzel, A. Fujimoto, J. W. Ager, E. E. Haller, J. Isoya, S. A. Lyon, M. L. Thewalt, and K. M. Itoh, *Phys. Rev. B* **82**, 121201 (2010).
- [32] V. Stepanov and S. Takahashi, *Phys. Rev. B* **94**, 024421 (2016).
- [33] N. Bar-Gill, L. Pham, A. Jarmola, D. Budker, and R. Walsworth, *Nat. Commun.* **4**, 1743 (2013).
- [34] K. Yamazaki, M. Kotani, and Y. Uchikawa, *IEEE Translation Journal on Magnetism in Japan* **7**, 519 (1992).
- [35] P. C. Maurer, G. Kucsko, C. Latta, L. Jiang, N. Y. Yao, S. D. Bennett, F. Pastawski, D. Hunger, N. Chisholm, M. Markham, D. J. Twitchen, J. I. Cirac, and M. D. Lukin, *Science* **336**, 1283 (2012).
- [36] L. T. Hall, J. H. Cole, and L. C. L. Hollenberg, *Phys. Rev. B* **90**, 075201 (2014).
- [37] N. Bar-Gill, L. Pham, C. Belthangady, D. Le Sage, P. Cappellaro, J. Maze, M. Lukin, A. Yacoby, and R. Walsworth, *Nat. Commun.* **3**, 858 (2012).
- [38] A. Dréau, J.-R. Maze, M. Lesik, J.-F. Roch, and V. Jacques, *Phys. Rev. B* **85**, 134107 (2012).
- [39] P. Jamonneau, M. Lesik, J. P. Tetienne, I. Alvizu, L. Mayer, A. Dréau, S. Kosen, J.-F. Roch, S. Pezzagna, J. Meijer, T. Teraji, Y. Kubo, P. Bertet, J. R. Maze, and V. Jacques, *Phys. Rev. B* **93**, 024305 (2016).
- [40] V. M. Acosta, E. Bauch, M. P. Ledbetter, A. Waxman, L.-S. Bouchard, and D. Budker, *Phys. Rev. Lett.* **104**, 070801 (2010).
- [41] K. Fang, V. M. Acosta, C. Santori, Z. Huang, K. M. Itoh, H. Watanabe, S. Shikata, and R. G. Beausoleil, *Phys. Rev. Lett.* **110**, 130802 (2013).
- [42] H. J. Mamin, M. H. Sherwood, M. Kim, C. T. Rettner, K. Ohno, D. D. Awschalom, and D. Rugar, *Phys. Rev. Lett.* **113**, 030803 (2014).
- [43] C. A. J. Ammerlaan and E. A. Burgemeister, *Phys. Rev. Lett.* **47**, 954 (1981).
- [44] R. L. Stamps, *J. Phys. D* **33**, R247 (2000).
- [45] J. Klauder and P. Anderson, *Phys. Rev.* **125**, 912 (1962).
- [46] W. M. Witzel, K. Young, and S. Das Sarma, *Phys. Rev. B* **90**, 115431 (2014).
- [47] V. V. Dobrovitski, A. E. Feiguin, D. D. Awschalom, and R. Hanson, *Phys. Rev. B* **77**, 245212 (2008).
- [48] G. Grimmett, *Probability and Random Processes* (Oxford University, New York, 2001).
- [49] V. V. Dobrovitski, A. E. Feiguin, R. Hanson, and D. D. Awschalom, *Phys. Rev. Lett.* **102**, 237601 (2009).
- [50] A. Jarmola, A. Berzins, J. Smits, K. Smits, J. Prikulis, F. Gahbauer, R. Ferber, D. Erts, M. Auzinsh, and D. Budker, *Appl. Phys. Lett.* **107**, 242403 (2015).

- [51] L. T. Hall, P. Kehayias, D. A. Simpson, A. Jarmola, A. Stacey, D. Budker, and L. C. L. Hollenberg, *Nat. Commun.* **7**, 10211 (2016).
- [52] T. Roskopf, A. Dussaux, K. Ohashi, M. Loretz, R. Schirhagl, H. Watanabe, S. Shikata, K. M. Itoh, and C. L. Degen, *Phys. Rev. Lett.* **112**, 147602 (2014).
- [53] D. A. Redman, S. Brown, R. H. Sands, and S. C. Rand, *Phys. Rev. Lett.* **67**, 3420 (1991).
- [54] A. Jarmola, V. M. Acosta, K. Jensen, S. Chemerisov, and D. Budker, *Phys. Rev. Lett.* **108**, 197601 (2012).
- [55] Now Scio Diamond Technology Corporation.
- [56] M. Schwander and K. Partes, *Diam. Relat. Mater.* **20**, 1287 (2011).
- [57] F. P. Bundy, H. T. Hall, H. M. Strong, and R. H. Wentorf, *Nature (London)* **176**, 51 (1955).
- [58] H. Sumiya and S. Satoh, *Diam. Relat. Mater.* **5**, 1359 (1996).
- [59] H. Kanda, *Braz. J. Phys.* **30**, 482 (2000).
- [60] C. B. Hartland, A study of point defects in CVD diamond using electron paramagnetic resonance and optical spectroscopy, Ph.D. thesis, University of Warwick, 2014.
- [61] A. M. Zaitsev, *Optical Properties of Diamond* (Springer-Verlag, Berlin, 2001), p. 502.
- [62] G. S. Woods, J. A. Van Wyk, and A. T. Collins, *Philos. Mag. B* **62**, 589 (1990).
- [63] L. Cywiński, R. M. Lutchyn, C. P. Nave, and S. Das Sarma, *Phys. Rev. B* **77**, 174509 (2008).